Supporting Information for

Water as a promoter and catalyst for dioxygen electrochemistry in aqueous and organic media

Jakub S. Jirkovský[†], Ram Subbaraman[†], Dusan Strmcnik[†], Katharine L. Harrison[‡], Charles E. Diesendruck[¶], Rajeev Assary[†], Otakar Frank[#], Lukáš Kobr[+], Gustav K. H. Wiberg[†], Bostjan Genorio[†,=], Justin G. Connell[†], Pietro P. Lopes[†], Vojislav R. Stamenkovic[†], Larry Curtiss[†], Jeffrey S. Moore[¶], Kevin R. Zavadil[‡] and Nenad M. Markovic[†*]

[†] Materials Science Division, Argonne National Laboratory, Argonne, IL, USA

[‡] Sandia National Laboratory, Albuquerque, NM, USA

[¶] University of Illinois at Urbana-Champaign, Urbana, IL, USA

+ Northwestern University, Evanston, IL, USA

#J. Heyrovsky Institute of Physical Chemistry, Prague, Czech Republic

= University of Ljubljana, Faculty of Chemistry and Chemical Technology, Ljubljana, Slovenia

1- Effect of water on dioxygen electrochemistry in DME-TBAPF$_6$ electrolytes

To explore the O$_2$ reduction reaction on Au(hkl) rotating disk electrodes in ultra-dry organic electrolytes, cyclic voltammetry experiments with varying sweep rates and rotation speeds are summarized in Figure S1a and S1b. A reversible O$_2$/O$_2^-$ redox couple centered at ~2.2 V is observed on both surfaces in dry DME. Further analysis of CV data and polarization curves confirms that the ORR takes place as a characteristic one-electron reduction of O$_2$ to O$_2^-$. Most significantly, these results demonstrate that the reaction is *not* a structure-sensitive process, confirming that binding of O$_2^-$ to Au surfaces is very weak. However, the systematic addition of water in these systems (Fig. S1c and S1d) reveals the structure-sensitivity of the ORR on Au surfaces, clearly showing that surface-sensitivity of water adsorption at the interface is the underlying effect. As there is no reason for the O$_2$ or O$_2^-$ interaction to be stronger in aqueous electrolytes on otherwise identical surfaces, the observed structure sensitivity for the ORR on gold single crystals in alkaline solutions may instead be related to the structure-sensitive adsorption of water molecules.
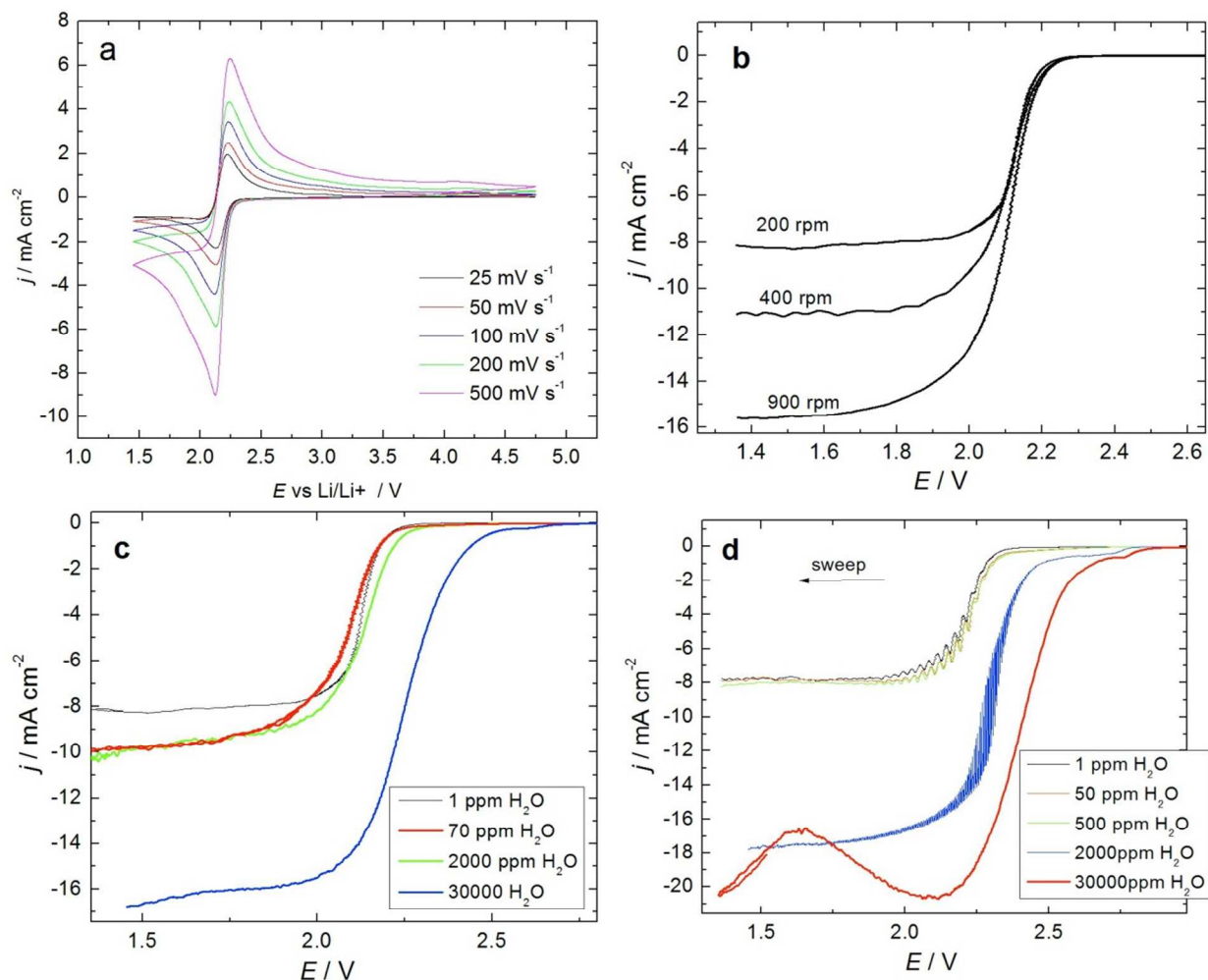
Figure S1. The effect of water on dioxygen electrochemistry. O_2 electrochemistry in ultra-dry DME/ TBAPF$_6$ on Au(111) by **a**, cyclic voltammetry at different sweep rates as indicated in the figure and **b**, polarization curves by RDE; rotation rate is indicated in the figure. Polarization curves in the same media but after addition of water recorded at **c**, Au(111) and **d**, Au(100). Sweep rate = 100 mV s^{-1}. The water content for panels c and d is indicated in the figure.
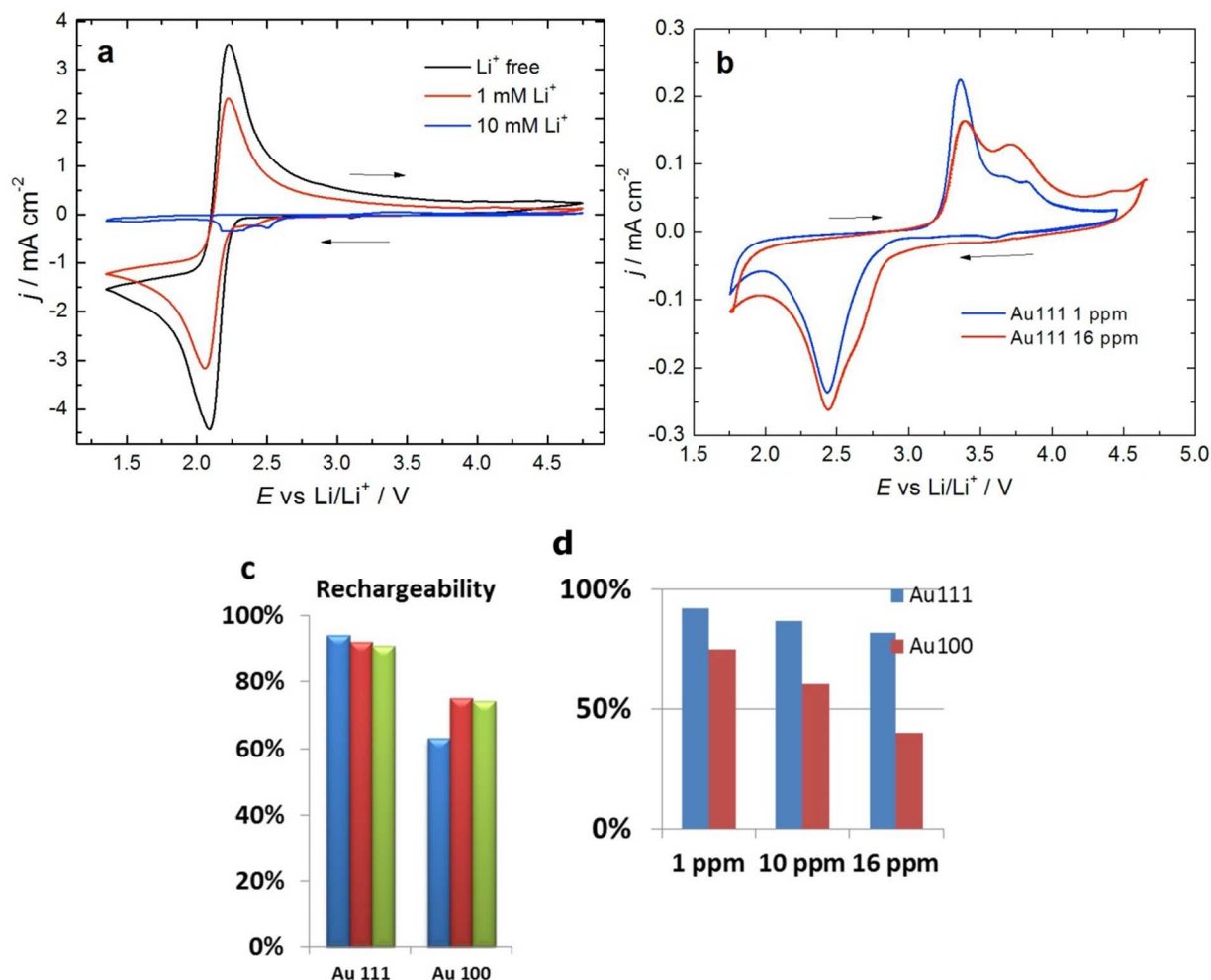
Figure S2. Dioxygen electrochemistry in aprotic media containing Li$^+$. O_2 Electrochemistry in O_2 saturated DME with supporting electrolyte consisting of **a**, TBAPF$_6$ and LiTFS and Au(111), the amount of Li is indicated in the figure. **b**, 0.3 M Li Triflate and 1 ppm of H$_2$O and 16 ppm of water on Au(111). **c**, Rechargeability in subsequent scans up to 20 cycles in dry electrolytes. **d**, Rechargeability as a function of water content between 1-16 ppm on Au(111) and Au(100).

Figure S2 illustrates the effect of Li$^+$ concentration on the rechargeability of Au (111), noting the very similar response as observed for Au (100) as shown in Figure 2 in the main text. In the presence of 1 mM Li$^+$, the most prominent features observed are the decrease of O_2^-/O_2 reversible peak intensity and the appearance of a small reduction current between 2.5 and 2.2 V.

These features point to an irreversible change in the O_2/O_2^- redox pair in the presence of Li^+. The degree of irreversibility increases with the concentration of Li^+. On the other hand, the addition of water does not change the voltammetry behavior for Au(111) as dramatically as what is observed for Au(100), most likely due the weaker adsorption of water on Au(111) surfaces. Note that the reversibility changes substantially due the presence of low levels of water in the electrolyte, an effect that is more significant for the Au(100) surface (Fig S2d).

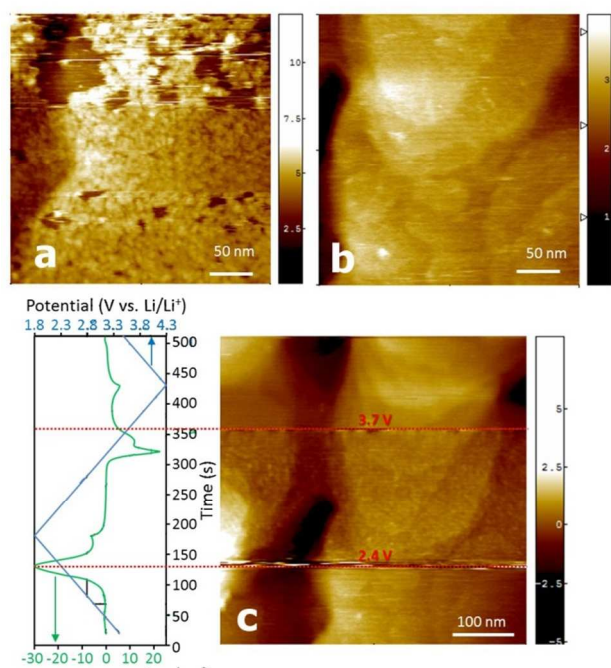## 2 – Characterization of surface deposits from Li-O$_2$ electrochemistry

Figure S3. In-situ AFM imaging of Au(111) in TEGDME/LiClO$_4$ saturated with O$_2$. a, Partial oxidation of the film shown in Fig. 2e now poised at 3.3 V imaged during an upward scan and showing the progression of dissolution between the nanoparticles, to hole formation, and finally complete consumption of sections of the film. **b,** Complete film oxidation is achieved at 3.8 V with the re-appearance of the general terrace and step structure shown in Fig. 2d. **c,** Film formation and subsequent dissolution monitored during cyclic voltammetry (10 mV·s^{-1}).

To understand the origin of the irreversibility of ORR in Li-containing solutions, *in situ* AFM experiments were carried out to characterize any morphological changes of the surface during

cyclic voltammetry experiments. In Figure S3 it is clear the formation of nanoparticles that are progressively consumed at 3.3V after their formation during the O_2 reduction sweep. Continuous imaging at 3.3V reveals formation of holes evolving to the removal of patches of the surface film formed from ORR. Complete film dissolution takes place only after 3.8 V. Note that the results on Figure S3c reveal the transition during a single scan from the typical surface terrace and steps morphology to the formation of nanoparticles and their consequent removal after the electrode potential is reversed again.

3- Assignment of the Raman bands

As discussed throughout the text, two main lithium-containing compounds – peroxide and superoxide – are expected to appear on the electrode surface during the ORR (at least in the early stages). The Li-O vibrations appear in the wavenumber range below 900 cm^{-1} and O-O υ_1 stretching vibrations appear between 700 and 1300 cm^{-1}. However, when explored in detail, the Raman response of the two materials (peroxide/superoxide) is fundamentally different. The first immediately observable differences between peroxide and superoxide vibrations are the distinctly grouped O-O vibrations. For peroxide (O_2^{2-}), the longer O-O distance of ~1.5 Å (in a singlet configuration)[1] results in band frequencies in the range of 700-900 cm^{-1}, whereas for superoxide (O_2^{1-}) the O-O vibration appears at 1050-1200 cm^{-1}, corresponding to the shorter bond length of ~1.34 Å[2]. As was shown previously[3], the frequencies of the O-O bands vary depending on the size of the Li_2O_2 clusters, especially due to minor changes in bond lengths for the particular structures[1]. The frequency of the O-O vibration in bulk Li_2O_2 was calculated at 800 cm^{-1} [1], which is approximately in accordance with the calculated results for the smaller clusters in ref. 2. The Li_2O_2 reference spectrum shown in Fig. S4C exhibits a sharp and intense peak at 785 cm^{-1} (note the absence of peaks in the 1100 cm^{-1} region as expected for a peroxide moiety). We can therefore assume that the peak observed at 785 cm^{-1} in the experimental spectra after 30 minutes of holding the potential of 2.5V with the addition of 40 ppm H_2O (Fig. 2f, main text, top spectrum) corresponds to the crystalline Li_2O_2. Alternatively, a rather uniform distribution of Li_2O_2 clusters (e.g. prevalently monomers) could be responsible for the observed band, since a broader cluster size distribution would in turn result in an equally broadened Raman peak enveloping all the particular, slightly varying O-O vibrations.

Supplementary Table S1 summarizes calculated Raman active vibrations for various clusters and environments of and LiO_2. Focusing on $(LiO_2)_x$ clusters in entries 2-5, we can see a large spread of the Li-O phonon frequencies from 740 down to 370 cm^{-1}, and a relatively steady position of the O-O vibration at ~1160 cm^{-1} (only the clusters in triplet states exhibit an additional O-O band at a different frequency). Bearing in mind that the formation of Li_xO_y takes place directly on the Au surface, the possible effects of gold on the Raman spectra of the products was examined. LiO_2 and Li_2O_2 may be adsorbed on gold which would cause additional shift of vibrations[4] due to changes in phonon density of states and also enhancement of some of the vibrations due to the SERS effect[5]. To simulate the effect of gold on the phonon frequencies of we have performed calculations with small Au-LiO_2 clusters as also shown in the Supplementary Table S1 on lines 6-10. As the first indication, the vibration of the Au_3-O_2^{1-} (entry 6) is downshifted by approximately 30 cm^{-1} compared to the "stand-alone" O_2^{1-} species (entry 1). Similarly, the downshift of the O-O stretching vibration is discernible also for Au-$(LiO_2)_x$ vs. $(LiO_2)_x$ clusters. However, there is a clear trend: in the presence of Au the band shifts back to higher wavenumbers with the size of LiO_2 clusters, probably reflecting the diminishing effect of gold. For the smallest comparable cluster gold causes a shift of the υ_1 band to lower wavenumbers by ~50 cm^{-1}.

As is clear from the calculated and experimental data, it is extremely difficult to distinguish between different deposits of LiO_2 and Li_2O_2 on (or off) gold. A narrower picture can be drawn, however, if one compares these calculations with experiments and theoretical Raman mode assignments based on infinite crystal structures. As stated above, both theoretical[1] and experimental studies[6] including our measurement (Fig. S4C) clearly show that crystalline Li_2O_2 should have only one very strong band at 785 cm^{-1} in the region under consideration (note we are not able to measure below 300 cm^{-1} due to an increased fluorescence caused by the electrolyte system). In the case of LiO_2 Raman bands, assignment becomes more complicated since LiO_2 is not a very stable species and thus bulk sources are scarce. However, several experiments in Ar and Ne matrices were performed to study deposits of LiO_2 by IR (mostly) and Raman, and accurate assignments were done by isotope labeling. These experiments clearly show that the O-O υ_1 stretching vibration is by far the strongest in the Raman spectra of LiO_2 (the peak observed at 1093 cm^{-1})[7]. Other Raman active bands are expected at ~700 cm^{-1} (υ_2 Li-O symmetric stretching vibration) and sometimes also at 500 cm^{-1}. These should be very weak, however, and

have never been clearly measured experimentally. On the other hand, several works[8] have shown a broad, complex structure in the spectra of Li or K superoxides at ~500 cm^{-1}, which were attributed to LiO_2 aggregates. Turning our attention back to the Supplementary Table S1, such a scenario seems to be plausible given the scattered range of Li-O vibrational frequencies for variously sized LiO_2 clusters and the quite steady position of the O-O vibration. Experimental work with a simultaneous deposition of LiO_2 and Au has also shown that redshifts due to the formation of LiO_2-Au clusters can be expected[4]. Little is known about the effect of Au surface plasmons in SERS and therefore it is difficult to predict which bands might get enhanced in the case of the adsorption of either LiO_2 or Li_2O_2 on gold. For LiO_2 formed in a more realistic environment on Au in acetonitrile, a band at 1130 cm^{-1} was observed[5]. Therefore we assign the 1130 cm^{-1} band in our spectra to the bulk LiO_2 that is, however, formed only after prolonged discharge under our experimental conditions.

We further attempt to resolve some of the issues with assignment of the Li-related vibrations by performing the same *in situ* Raman experiments as in Figure 2f (main text) with $^6LiClO_4$ as shown in Fig. S4B. The lower mass of the ^6Li isotope (compared to ^7Li) causes a certain phonon blueshift depending on the contribution of lithium atom(s) to the particular vibration. Hence, concerning the species in question and the measurable Raman shift range, only Li-O vibrations in LiO_2 are expected to shift with the Li isotope change. These are indicated in the Figure S4B. In LiO_2 the substitution of ^7Li by ^6Li should induce an upshift of ~15 cm^{-1} for the band around ~500 cm^{-1} and of ~50 cm^{-1} for the band at 700 cm^{-1}. As shown in the spectra in Figure S4B, the band at 700 cm^{-1} does indeed shift to 750 cm^{-1} and therefore we can assign this band to the surface adsorbed LiO_2. A minute change in the mass of the band at 500 cm^{-1} can be traced in the spectra as well, however, the band is very broad and the expected Li isotope shift is too small to make any sound assignment at this point. No shift caused by ^6Li substitution is expected for the O-O υ_1 band for it is a purely oxygen-involved vibration. We can hypothesize that the reason for observing the Li-O bands in our case (in contrast to previous work) might be the presence of Au surface plasmon enhancement. Consequently, we expect that the band at 1080 cm^{-1} may also belong to the Au-adsorbed LiO_2 (O-O stretch) *via* the Au induced redshift of ~50 cm^{-1} with respect to the bulk LiO_2 (1130 cm^{-1}). This assignment is also consistent with the weak time dependence of these peaks where formation of a thicker layer of LiO_2 might lead to their masking.
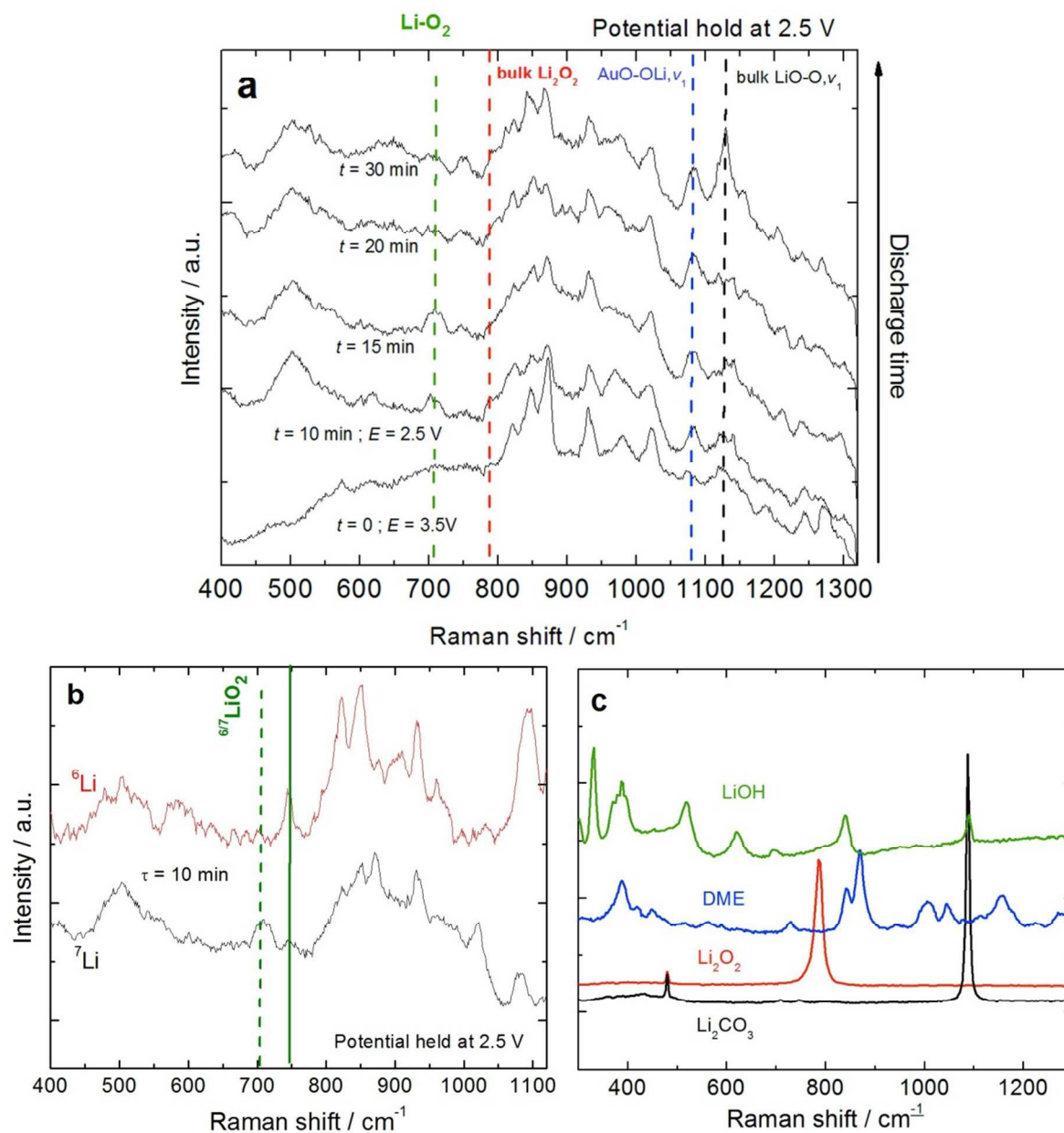
Figure S4. Raman spectroscopy of an electrochemical interface. a, In-situ Raman spectroscopy in O_2 saturated DME, 0.3M $LiClO_4$ at roughened gold surface, water content = ~1ppm. Potential was held at 2.5V. Spectra were collected subsequently and each collection took 1 minute, The time of the discharge process until each shown spectrum was measured is indicated in the Figure. **b**, DME, 0.3M $^7LiClO_4$ (black) and $^6LiClO_4$ (red) of roughened gold surface. Potential was held at 2.5V. Each spectrum required 1 minute for collection. The vertical lines are added to guide the eye. **c**, Reference spectra for selected relevant species were measured individually (as a clean substance).

Table S1: Computed unscaled Raman stretching vibrations and intensities of various lithium-oxide clusters at the B3LYP/6-31+G(d) level of theory.

Entry	Species	Electronic state	Peak position (Intensity)	
			Li-O	O-O
1	O_2^{1-}	Doublet		1172 (34)
2	$^a(LiO_2)_1$	Doublet	740 (14)	1161 (13)
3	$^a(LiO_2)_2$	Triplet	513 (6)	1161 (14), 1213 (19)
4	$^a(LiO_2)_3$	Doublet	442 (2)	1167 (31)
5	$^a(LiO_2)_4$	Triplet	373 (23), 492 (15)	1055 (40),1157 (41)
6	$(Au_3\text{-}O_2^{1-})$	Singlet		1144 (159)
7	$(Au_3\text{-}(LiO_2)_1)$	Singlet	667 (42)	
8	$Au_3\text{-}(LiO_2)_2)$	Doublet	430 (303), 831 (263)	1106 (174)
9	$Au_3\text{-}(LiO_2)_3)$	Singlet	596 (62)	1150 (93)
10	$Au_3\text{-}(LiO_2)_4)$	Doublet	629 (523), 847 (888)	1157 (53), 1163 (66)

Notes: ^{a} optimized structures from Ref 9

We note that the band at 1080 cm^{-1} in water-containing electrolytes will be overlapped by the much stronger band of Li_2CO_3. We expect that Li_2CO_3 can be formed from DME decomposition products and from reactions with Li_2O_2 or LiO_2. Regarding the decomposition products, it is interesting to note a series of additional peaks above 1150 cm^{-1} that are observed only in 'wet' electrolytes (40ppm). These peaks cannot be assigned to Li formate and indicate that the DME decomposition in the presence of Li is different than in TBA$^+$-based electrolytes

(Figure 2), possibly due to different reaction intermediates (LiO_2, Li_2O_2, HO_2, HO_2^-). The decomposition is strongly enhanced in the presence of water.

4- Calculations for reaction energies of Li-O$_2$ system at the interface

In Table S2 the reaction free energies of model systems for reaction scheme in Figure 3 are presented. Entries 1-2 correspond to the formation of LiO_2 for step 1$\rightarrow$2 in Figure 4. Entry 3 corresponds to formation of an O_2Li-OH_2 complex from LiO_2 and H_2O in step 2$\rightarrow$3 in Figure 4. Entry 4 corresponds to addition of O_2^{1-} to the O_2Li-OH_2 complex in step 3$\rightarrow$4 in Figure 4 and entry 5 shows the energy for breaking the OH bond of water. Note that this is much more favorable than when LiO_2 is not present (entries 9 and 10), consistent with experiment. Entry 6 corresponds to addition of an electron to the $O_2Li-OH_2-OO^-$ complex in step 4$\rightarrow$5 in Figure 4. Entries 7 and 8 correspond to addition of Li cations to the $O_2Li-OH^--OOH^-$ complex in step 5$\rightarrow$6 in Figure 4. Entries 11 and 12 show the energies for model systems of the aqueous system for the interaction of OH radical with H_2O. Note that entries 9-12 indicate the breaking of the OH bond in H_2O to be much more favorable in the presence of OH radical, which approximates the function of OH_{ad} in Figure 1.

Table S2. Reaction free energies for reaction schemes in Figures 2 and 4.

Entry	Reaction	G4MP2 (298 K), eV		
		ΔG(gas)	ΔG^a(acetone)	ΔG^b (water K)
1	$O_2 + 1e \rightarrow O_2^{1-}$	-0.41	-3.15 (1.91V^c)	-4.20 (2.96 V^c)
2	$Li^+ + O_2^{1-} \rightarrow LiO_2$	-7.30	-1.35	-0.40
3	$(LiO_2) + H_2O \rightarrow (O_2Li-OH_2)$	-0.37	-0.21	-0.22
4	$(O_2Li-OH_2) + O_2^- \rightarrow (O_2Li-OH_2-OO^-)$	-1.83	-0.52	+0.20
5	$(O_2Li-OH_2) + O_2^- \rightarrow (O_2Li-OH^-) + OOH$	-0.66	+0.30	+0.82
6	$(O_2Li-OH_2-OO^-)^d + 1e- \rightarrow (O_2Li-OH^--OOH^-)$	+2.74	-3.15 (1.91 V)	-4.43 (3.19 V)
7	$(LiO_2-OH^--OOH^-) + Li^+ \rightarrow (LiO_2-H_2O-LiO_2^-)$	-10.68	-1.53	-0.47
8	$(LiO_2-H_2O-LiO_2^-) + Li^+ \rightarrow (LiO_2-H_2O-Li_2O_2)$	-7.43	-1.72	-1.04
9	$O_2^{1-} + H_2O \rightarrow OH^- + OOH$	+1.47	+1.13	0.72
10	$O_2^{1-} + H_2O \rightarrow OH + OOH^-$	+2.26	+2.24	+2.00
11	$OH(radical) + H_2O \rightarrow (OH-H_2O)$ radical	+0.11	+0.14	+0.17
12	$(OH-H_2O)$ radical + $O_2(1-) \rightarrow (OH-OH^-) + OOH$ radical	+0.28	+0.55	+0.65

^{a}: Solvation energy (acetone dielectric) computed at the B3LYP/6-31G(2df,p) level of theory is added to the G4MP2 gas phase free energy. ^{b}: Solvation energy (water medium) computed at the B3LYP/6-31G(2df,p) level of theory is added to the G4MP2 gas phase free energy, ^{c}: redox potential with respect to Li/Li+ reference electrode, ^{d}: triplet.

Supplementary References

(1)   Lau, K.C.; Assary, R.S.; Redfern, P.; Greeley, J.; Curtiss, L.A. *J. Phys. Chem. C* **2012**, 116, 23890-23896.

(2)   Yang, J.; Zhai, D.; Wang, H-H.; Lau, K.C.; Schuleter, J.A.; Du, P.; Myers, D.J.; Sun, Y-K.; Curtiss, L.A.; Amine, K. *Phys. Chem. Chem. Phys.* **2013**, 15, 3764-3771.

(3)   Kidd, G. K.; Mantsch, H. H. *J. Mol. Spectrosc.* **1981**, 85, 375-389.

(4)   Wang, X.; Andrews, L. *J. Phys. Chem. A* **2001**, 105, 5812-5822.

(5)   Peng, Z.; Freunberger, S.A.; Hardwick, L.J.; Giordani, V.; Bardé, F.; Novák, P.; Graham, D.; Tarascon, J-M.; Bruce, P.G. *Angew. Chem. Int. Ed.* **2011**, 50, 6351 – 6355.

(6)   Eysel, H.H.; Thym, S. *Z. Anorg. Allg. Chem.* **1975**, 411, 97-102.

(7)   Smardzewski, R.R.; Andrews, L. *J. Chem. Phys.* **1972**, 57, 1327-1333.

(8)   Hunter-Saphir, S. A.; Creighton, J. A. *J. Raman Spectrosc.* **1998**, 29, 417-419.

(9)   Das, U.; Lau, K.C.; Redfern, P.C.; Curtiss, L.A. *J. Phys. Chem. Lett.* **2014**, 5, 813-819.